Mechanism of the Zonal Displacements of the Pacific Warm Pool: Implications for ENSO

J. Picaut,* M. Ioualalen, C. Menkes, T. Delcroix, M. J. McPhaden

The western equatorial Pacific warm pool is subject to strong east-west migrations on interannual time scales in phase with the Southern Oscillation Index. The dominance of surface zonal advection in this migration is demonstrated with four different current data sets and three ocean models. The eastward advection of warm and less saline water from the western Pacific together with the westward advection of cold and more saline water from the central-eastern Pacific induces a convergence of water masses at the eastern edge of the warm pool and a well-defined salinity front. The location of this convergence is zonally displaced in association with El Niño–La Niña wind-driven surface current variations. These advective processes and water-mass convergences have significant implications for understanding and simulating coupled ocean-atmosphere interactions associated with El Niño–Southern Oscillation (ENSO).

The equatorial Pacific surface waters are characterized by a regular increase of sea-surface temperature (SST) from the South American coast to near the international date line and then a nearly constant and high SST all the way to the Philippine coast (Fig. 1). In addition, the surface salinity of these waters differs, with more saline water in the central equatorial Pacific and less saline water in the western equatorial Pacific. This surface distribution is reflected in the thermocline depth along the equator, which gradually increases from near the surface at the Galápagos Islands to a depth of 100 to 150 m around the date line and then remains nearly constant further to the west (*1*). In the western tropical Pacific, the waters above the thermocline are well mixed, with temperatures >28°C; this constitutes the Pacific warm pool, which is fundamental to the climate of the Earth because it drives the world's most intense atmospheric convection (*2, 3*). In the scientific plan for the Tropical Ocean and Global Atmosphere–Coupled Ocean-Atmosphere Response Experiment (TOGA-COARE) (*3*), it was shown that the simultaneous zonal migrations of warm pool SST and atmospheric convection are essential features of ENSO. The atmospheric convection and associated low-level convergent winds follow the interannual eastward and westward migration of the warm pool (*4*), during the El Niño warm phase and the La Niña cold phase of ENSO, respectively (Fig. 1). It was also suggested (*3*) that the warm pool may be associated with the zonal convergence of the oceanic circulation in the western tropical Pacific, and that low surface salinity in the western Pacific may have important implications for ENSO (*5*). With the use of four data sets and three classes of ocean models, we demonstrate the dominance of zonal advection in the zonal migration of the eastern edge of the warm pool. This is evidenced through the discovery of a zonal convergence of water masses and a well-defined salinity front at the eastern edge of the warm pool, which together move along the equator in phase with the Southern Oscillation.

Most of the data presented in this study were collected during the 1985–94 TOGA decade. The model outputs cover the period 1982–94, which includes the 1982–83 El Niño (the most intense of the 20th century), the 1986–89 El Niño–La Niña sequence, and the extended period of warm El Niño conditions spanning 1991–94. Whenever possible, the data and model outputs were transposed on a common grid (5° longitude, 1° latitude, 5-day). The longest data set is based on four Tropical Atmosphere-Ocean (TAO) moored buoys at the equator and 156°E, 165°E, 140°W, and 110°W (*6*); it is defined as the TAO field and consists of near-surface current measurements which were interpolated along the equator during 1986–94. Another near-surface current field (*7*), defined as the buoy field, was built on a bimonthly basis from mid-1988 to the end of 1993 from a combination of data from more than 1000 drifting buoys and near-surface currents from the four equatorial TAO moored buoys. Two additional surface-current fields were derived from satellite altimetry measurements: GEOSAT over the November 1986–February 1989 period (*8*) and TOPEX/POSEIDON over the September 1992–December 1994 period (*9*). Three different model outputs were used: (i) the Cane and Patton linear multimode model (*10*) forced by the Florida State University (FSU) wind stress over the 1982–94 period, (ii) the Gent and Cane nonlinear model forced by the FSU wind stress and the heat flux deduced from an advective atmospheric mixed-layer model (*11*) over the 1982–94 period, and (iii) the three tropical oceans Laboratoire d'Océanographie Dynamique et de Climatologie (LODYC) high-resolution ocean general circulation model (*12*) forced by the wind stress, heat flux, and rainfall derived from the Météo-France atmospheric global circulation model over the 1986–94 period.

Following previous studies (*13–15*) suggesting the importance of zonal advection in the ENSO displacement of the eastern

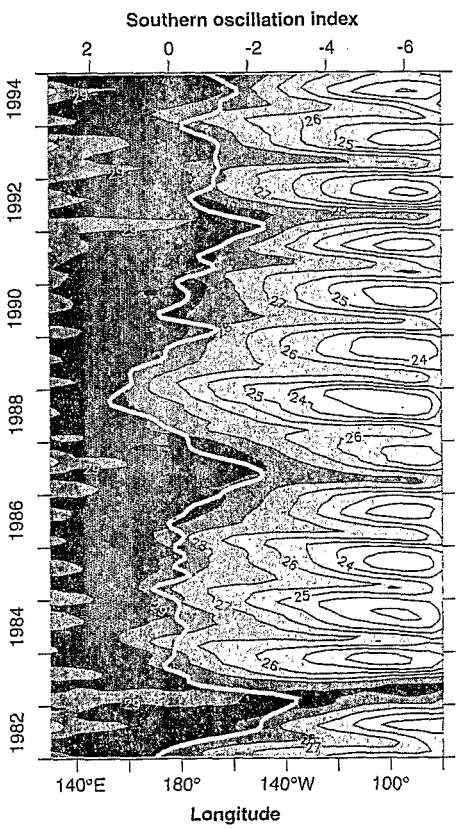

Fig. 1. Longitude-time distribution of the 4°N–4°S averaged SSTs. The Southern Oscillation Index (SOI, upper scale, normalized difference between the sea level pressure anomalies at Tahiti, French Polynesia, and Darwin, Australia), filtered with a 6-month Hanning filter, is superimposed as a thick white line. The SOI is closely related to SST, surface wind, and atmospheric convection changes in the tropical Pacific. Note the very good phase agreement between the SOI and the El Niño–La Niña migration of the eastern edge of the warm pool.

J. Picaut, M. Ioualalen, T. Delcroix, Groupe SURTROPAC, Institut Français de Recherche Scientifique pour le Développement en Coopération (ORSTOM), BP A5, 98848, Nouméa, New Caledonia.
C. Menkes, Centre de Recherche Océanographique, ORSTOM, Abidjan, Ivory Coast.
M. J. McPhaden, Pacific Marine Environmental Laboratory, National Oceanic and Atmospheric Administration, Seattle, WA 98115, USA.
*To whom correspondence should be addressed. E-mail: picaut@noumea.orstom.nc

edge of the warm pool, all surface-current fields were used to compute the zonal displacements of water mass transported by the 4°N–4°S averaged currents. These displacements were tracked with hypothetical drifters that were assumed to move with the 4°N–4°S averaged zonal currents. The range of latitude between 4°N and 4°S was chosen because it is in the equatorial wave guide where the largest SST and near-surface zonal current anomalies are found (*7*, *16*). The resulting trajectories of water mass were compared to the displacement of the eastern edge of the warm pool (more specifically, the 29°C isotherm) which, for consistency, was inferred from the observed SST (*17*) for both observational (Fig. 2) and model-derived (Fig. 3) results.

The use of hypothetical 4°N–4°S drifters in this study requires some clarification. In the eastern and central equatorial regions, the westward displacements induced by the trade winds are subject to surface Ekman divergence that results, on average, in a 5 cm/s poleward meridional current in either hemisphere (*18*); thus, real surface drifters launched in the equatorial band will leave this band of latitudes in less than 3 months while traveling 1000 or 2000 km toward the warm pool. However, even if a single parcel of surface water originating from the eastern equatorial Pacific rarely reaches the eastern edge of the warm pool directly, there is a nearly continuous westward transport of water mass in the upper layer toward the warm pool along the equator (*19*). It is this transport that we are emphasizing with our hypothetical drifters because the effects of divergent meridional surface currents near the equator tend to cancel out when considering averages over the latitudinal band between 4°N and 4°S. Similarly, in the warm pool, with westerly wind bursts, there is a tendency for Ekman convergence and eastward transport of water mass toward the central equatorial Pacific. As in the eastern and central Pacific, averaging currents over 4°N–4°S emphasizes the zonal rather than the meridional velocity field and associated displacements. Thus, the trajectories of the hypothetical drifters effectively highlight the zonal displacements of water masses along the equatorial band resulting from the integration in space and time of the surface currents within 4°N–4°S.

When moved by the buoy field, a 4°N–4°S hypothetical drifter launched on the eastern edge of the warm pool in mid-1988 remained close to this edge up to the end of 1993 (Fig. 2). Hypothetical drifters launched east of the corresponding trajectory always converged within 1 to 3 years toward the original trajectory; similar convergence happened with hypothetical drifters launched a little west of the main trajectory, although not systematically. When moved by the TAO field, a hypothetical drifter launched on the eastern edge of the warm pool in early 1986 followed its zonal migration associated with the 1986–87 El Niño. Then, because of the strong westward surface current associated with the 1988–89 La Niña, the hypothetical drifter moved westward past the westernmost TAO moored buoy. A second hypothetical drifter, launched at the end of 1989 when the current started going eastward again, stayed close to the eastern edge of the warm pool during the extended 1991–94 El Niño. In the same way as with the buoy field, drifters launched a little west and east of the two previous TAO trajectories usually converged to these trajectories after 1 to 3 years. Finally, the GEOSAT- and TOPEX/POSEIDON–derived trajectories both remained close to the eastern edge of the warm pool, the former during the 1986–89 El Niño–La Niña sequence (*15*) and the latter during the extended period of El Niño conditions in 1992–94.

These results based on observations are surprisingly coherent considering the resemblance between the trajectories and warm-pool zonal migration, especially bearing in mind the intrinsic deficiencies of each current field (less than 100 drifting buoys per year in the equatorial band, interpolation in longitude between widely separated moored buoys, and altimetry-derived surface currents constrained by geostrophy). We thus confirm the suggestion of our previous studies (*14*, *15*), which are based on the more restrictive time period of 1986–89 and limited observed data sets, that zonal advection of temperature is the dominant mechanism in determining the zonal migration of the eastern edge of the warm pool over the entire period 1986–94. An exception to this conclusion occurred during the 1988–89 La Niña, when strong westward currents yielded trajectories that were either too westward (using the buoy field) or that escaped from our study area (using the TAO field). At this time, processes other than zonal advection probably have some effect on SST.

Each current field, simulated by the three different models, leads to its own single trajectory (Fig. 3). In the case of the linear model, the mean westward shift of its trajectory, compared to observed trajectories (Fig. 2) and the eastern edge of the warm pool, is most probably due to the simplified physics of the model, in particular, the exclusion of nonlinear terms. As suggested by previous studies (*20*), the ad-

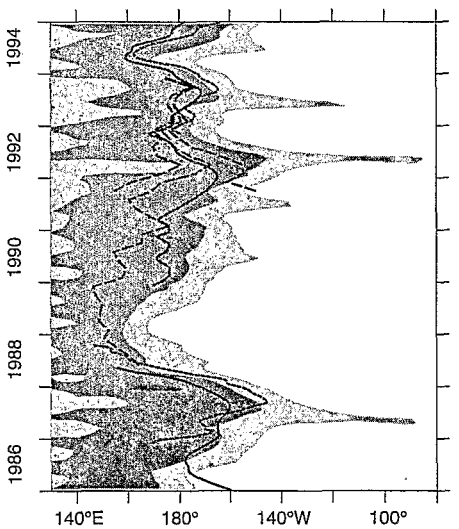

Fig. 2. Trajectories of hypothetical drifters moved by 4°N–4°S averaged surface zonal currents, obtained from the TAO field (solid line), the buoy field (long dashed line), and the altimetry field (GEOSAT and TOPEX/POSEIDON) (short dashed line). Superimposed are the observed SSTs of Fig. 1, restricted for clarity to values higher than 28°C, with a shading at increments of 1°C. Also shown is an example of zonal convergence to the main trajectory of two additional 4°N–4°S drifters, launched in boreal fall 1991 into the current buoy field (the additional long dashed lines around 1992).

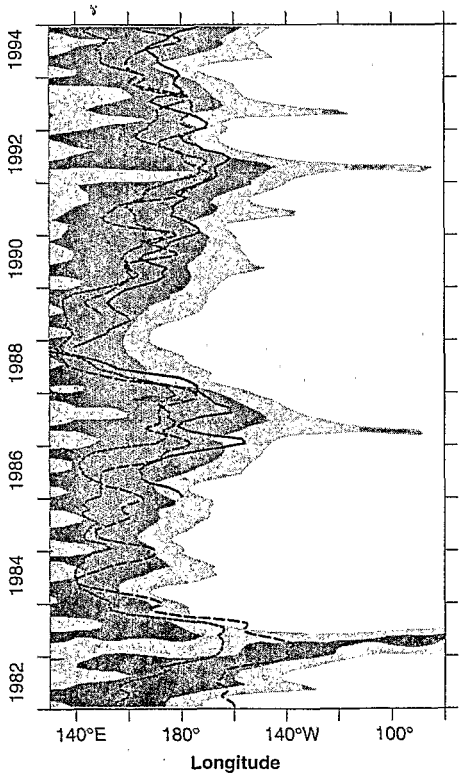

Fig. 3. Trajectories of hypothetical drifters moved by 4°N–4°S averaged surface zonal current fields, simulated from the LODYC (solid line), the Gent and Cane (long dashed line), and the linear models (short dashed line). Superimposed are the observed SSTs of Fig. 1, restricted for clarity to values higher than 28°C, with a shading at increments of 1°C.

dition of these terms would result in an increase of eastward (a decrease of westward) equatorial currents. This is confirmed by the trajectories, obtained from both the nonlinear Gent and Cane and LODYC models, which are similar and closely follow the eastern edge of the warm pool. Note that the LODYC trajectory exits from our study area during the 1988–89 La Niña, as does the trajectory derived from the TAO field (Fig. 2). Overall, the set of single trajectories derived from the three models tracks the eastern edge of the warm pool reasonably closely. Similar to the results obtained with the observed current fields (Fig. 2), each single trajectory results from the zonal convergence of 4°N–4°S hypothetical drifters launched west and east of the main trajectory, as shown with the LODYC model (Fig. 5). The convergence of water masses on the eastern edge of the warm pool results from the existence, in observations and models, of a quasi-permanent westward surface flow in the eastern equatorial Pacific and frequent eastward surface flows in the western equatorial Pacific under the influence of westerly wind bursts and penetrating monsoon winds.

Given the presence of rainfall-induced fresh water in the warm pool and more saline water to the east, the zonal convergence of water masses within the equatorial band results in a well-marked salinity front and therefore in a density front along the equator. This salinity front is evident in the upper 50 to 70 m in numerous space- and time-limited observational studies (*21–23*). The front is also apparent in sea-surface salinity observations obtained mainly from a ship-of-opportunity network (Fig. 4), although with some smearing due to interpolation between four main cross-equatorial shipping lanes (*24*). This salinity front also appears in the LODYC model output, with a one-unit difference over less than 10° longitude (Fig. 5). In this model simulation, the front is remarkably close to the 4°N–4°S main drifter trajectory, and it is also very close to the simulated eastern edge of the warm pool (*25*). In Fig. 5, pairs of hypothetical drifters launched east and west of the main trajectory converge into this trajectory, and so illustrate the concept of the formation of this salinity front through surface current and water mass convergence. Because the main trajectory is moved only by zonal currents, the good correspondence between the trajectory and the salinity front indicates that zonal advection of salinity is the main mechanism for the interannual zonal displacements of this front, much as zonal advection of temperature is mainly responsible for the interannual zonal displacements of the eastern edge of the warm pool.

In contrast to salinity, there is no well-marked temperature front along the equator. The net heat flux and the intensity of the equatorial upwelling both decrease from the eastern to the central equatorial Pacific (*26*), and the upwelled waters are mixed with the surrounding warmer surface waters during the course of their westward transport. These processes result in a progressive SST warming from east to west, and the salinity front clearly delineates the separation between a well-defined zonal SST gradient in the east and an almost zero zonal SST gradient in the warm pool. Because the SST gradient along the equator is important in driving the surface easterly winds (*27*), the aforementioned separation (that is, the eastern edge of the warm pool) and its zonal displacement are crucial for the ENSO ocean atmosphere–coupled system, because they are tied to the wind convergence and associated convection (*4*).

Because the salinity front is induced by current convergence, it is situated in a region of very weak or null zonal currents, which, together with the corresponding density front, restrain the heat exchange between the warm pool and the equatorial region further east. The convergence of surface currents and water masses not only results in the formation of the salinity front but also in the subduction of more saline water from the central equatorial Pacific below the less saline water of the western Pacific (*28*). This creates the underlying barrier layer in the equatorial band, which obstructs entrainment of the colder and saltier water into the surface layer (*5*). The warm pool, which is composed of low-density fresher and warm water, floats above the high-density cold and saltier water; therefore, it can be easily displaced zonally by wind-driven currents, as the momentum is trapped in a shallow mixed layer (*28, 29*). All of this explains why the warm pool is somewhat isolated from the remaining equatorial Pacific and why there is such a good agreement among the ENSO displacements of the eastern edge of the warm pool, of the zonal convergence of water masses, and of the zonal salinity front.

Our results have important implications for understanding coupled ocean-atmosphere variations associated with ENSO (*30*). Displacements of the eastern edge of the warm pool along the equator are the reason for central equatorial Pacific SSTs to vary between 26° and 30°C on ENSO time scale (Fig. 1). Given that an SST of 28°C is the threshold for formation of organized atmospheric convection, the resulting convection (and therefore associated surface winds and rainfall) follows the zonal displacement of the eastern edge of the warm pool (*4*) and leads to global ENSO atmospheric teleconnections (*2*). In contrast, in the oceanic cold regions further east, larger ENSO SST variations have much weaker global climatic impacts (*31*). As a consequence, zonal advection together with convergence of surface currents and water masses in the central equatorial Pacific are key factors in maintaining ocean-atmosphere interactions on ENSO time scales. Ocean and coupled ocean-atmosphere

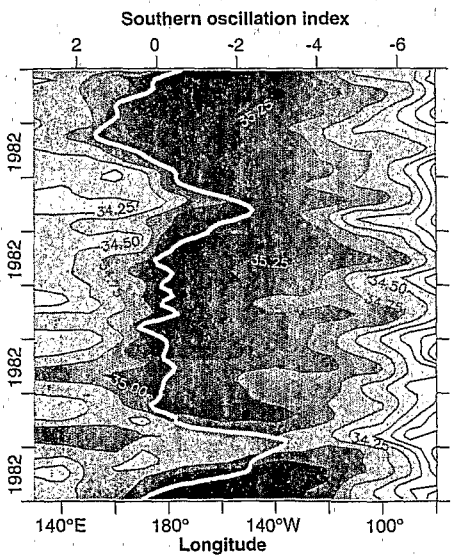

Fig. 4. Longitude-time distribution of 4°N–4°S averaged sea-surface salinity obtained from a ship-of-opportunity network and sparse hydrological data. The SOI is superimposed as a thick white line, as in Fig. 1.

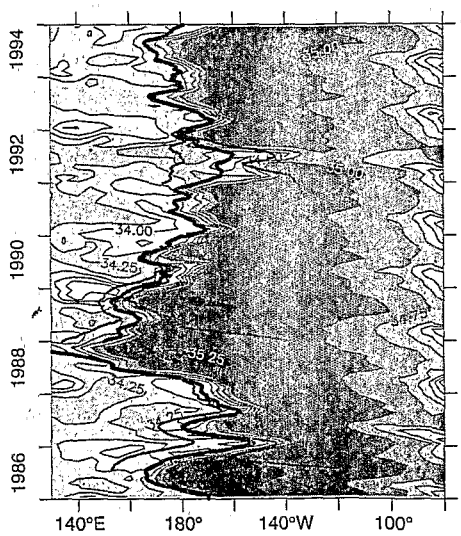

Fig. 5. Longitude-time distribution of 4°N–4°S averaged sea-surface salinity, as simulated by the LODYC model. The trajectories of hypothetical drifters moved by the LODYC-simulated 4°N–4°S averaged zonal current are superimposed (thick solid line). Also shown are examples of several pairs of drifters converging into the main trajectory that closely follows the salinity front (additional lines around 1987, 1989, and 1992).

models must therefore accurately reproduce these processes to correctly simulate ENSO.

With the eastern edge of the warm pool moved back and forth along the equator by zonal currents during La Niña and El Niño, the variation of zonal currents in the equatorial central Pacific controls the basic time scale of the ENSO cycle. In the central equatorial Pacific, these zonal currents are generated by local wind forcing, equatorial Kelvin and first meridional mode Rossby waves, and their reflections on the eastern and western ocean basin boundaries (*8*, *15*, *32*, *33*). Eastern boundary reflections and resulting first meridional mode Rossby waves (enhanced along their propagation by wind forcing further west) were observed to shift the 1986–87 El Niño into the 1988–89 La Niña through zonal advection of the eastern edge of the warm pool (*15*). Therefore, we propose for the oscillatory nature of ENSO an extension of the original delayed-action oscillator theory (*34*, *35*). In this extension, the predominant ocean-atmosphere coupling is situated in the central equatorial Pacific, as observed (*36*). In addition, reflections of equatorial waves at both eastern and western boundaries are important in shifting the phase of ENSO (*33*). In this scenario, zonal advective processes, as determined by us, are fundamental in establishing the ENSO time scale.

REFERENCES AND NOTES

1. L. Lemasson and B. Piton, *Cah. ORSTOM Ser. Oceanogr.* **6**, 39 (1968).
2. N. E. Graham and T. P. Barnett, *J. Clim.* **8**, 544 (1995).
3. World Climate Research Program, *WMO Publ. Ser. 3 Addendum* (Geneva, 1990).
4. C. Fu, H. F. Diaz, J. O. Fletcher, *Mon. Weather Rev.* **114**, 1716 (1986).
5. R. Lukas and E. Lindstrom, *J. Geophys. Res.* **96**, 3343 (1991).
6. M. J. McPhaden, *Oceanography* **6**, 36 (1993).
7. C. Frankignoul, F. Bonjean, G. Reverdin, *J. Geophys. Res.* **101**, 3629 (1996).
8. T. Delcroix, J.-P. Boulanger, F. Masia, C. Menkes, *ibid.* **99**, 25093 (1994).
9. C. Menkes, J.-P. Boulanger, A. J. Busalacchi, *ibid.* **100**, 25087 (1995).
10. M. A. Cane and R. J. Patton, *J. Phys. Oceanogr.* **14**, 1853 (1984).
11. R. R. Murtugudde, R. Seager, A. J. Busalacchi, *J. Clim.* **9**, 1795 (1996).
12. P. Delecluse, G. Madec, M. Imbard, C. Levy, *Rapp. Interne LODYC 93/05* (Université de Paris VI, Paris, 1993).
13. A. E. Gill, *J. Phys. Oceanogr.* **13**, 586 (1983).
14. M. J. McPhaden and J. Picaut, *Science* **250**, 1385 (1990).
15. J. Picaut and T. Delcroix, *J. Geophys. Res.* **99**, 18393 (1995).
16. T. Delcroix, G. Eldin, M.-H. Radenac, J. M. Toole, E. Firing, *ibid.* **97**, 5423 (1992).
17. R. W. Reynolds and T. M. Smith, *J. Clim.* **8**, 1571 (1995).
18. P. M. Poulain, *J. Phys. Oceanogr.* **23**, 601 (1993).
19. K. Wyrtki, *ibid.* **5**, 572 (1975).
20. S. G. H. Philander and R. C. Pacanowski, *J. Geophys. Res.* **85**, 1123 (1980).
21. L. Mangum *et al.*, *ibid.* **95**, 7279 (1992).
22. Y. Kuroda and M. J. McPhaden, *ibid.* **98**, 4747 (1993).
23. J.-R. Donguy, *Prog. Oceanogr.* **34**, 45 (1994).
24. T. Delcroix and C. Hénin, *J. Geophys. Res.* **96**, 22135 (1991).
25. C. Maes, thesis, Université de Paris VI, Paris (1996).
26. S. K. Esbensen and Y. Kushnir, *Oregon State University Report No. 21* (1981).
27. R. S. Lindzen and S. J. Nigam, *J. Atmos. Sci.* **44**, 2418 (1987).
28. Vialard and Delecluse have found, from a detailed analysis of the LODYC ocean general circulation model, two regions of barrier layer formation: one in the equatorial band in relation to the zonal convergence of water masses discussed in this paper and another further south in relation to zonal and meridional flows (J. Vialard and P. Delecluse, in preparation.
29. D. Chen, A. J. Busalacchi, L. M. Rothstein, *Proc. Int. Conf. TOGA Prog.*, World Meteorological Organization/TD No. 717, 675 (1995).
30. Moreover, it is likely that water-mass convergence and zonal advection in the equatorial Pacific have significant biological implications at the level of primary production and fish resource distributions (for example, the tuna fishery is known to be very important about the warm pool).
31. T. N. Palmer and D. A. Mansfield, *Nature* **310**, 483 (1984).
32. J.-P. Boulanger and L. Fu, *J. Geophys. Res.* **101**, 16361 (1996).
33. The equatorial Kelvin and first meridional mode Rossby waves, which are probably most important for ENSO (*15*, *34*, *35*), propagate along the equator eastward and westward, respectively. Both have surface zonal current extrema at the equator. They can be generated by reflections on western and eastern boundaries, respectively, of equatorial waves originating from the same wind forcing in the central equatorial Pacific. These reflected equatorial waves would result, after some delay, in surface zonal currents opposed to the direction of the zonal currents forced by the original wind. This delayed-action effect on surface zonal currents may be the reason for a gradual shift in the direction of the zonal advection of the eastern edge of the warm pool and therefore for the phase shift of ENSO.
34. D. S. Battisti, *J. Atmos. Sci.* **45**, 2889 (1988).
35. P. S. Schopf and M. J. Suarez, *J. Phys. Oceanogr.* **20**, 629 (1990).
36. N. J. Mantua and D. S. Battisti, *J. Clim.* **8**, 2897 (1995).

37. We thank the following persons for providing data or model outputs: F. Bonjean, P. Delecluse, C. Frankignoul, E. Hackert, C. Lévy, R. Murtugudde, J. J. O'Brien, G. Reverdin, and R. W. Reynolds. We also thank F. Masia for programming assistance, M.-J. Langlade and H. P. Freitag for additional programming support, and J. Vialard for discussions. Supported by ORSTOM, Programme National de Télédétection Spatiale, and the NOAA Office of Global Programs (M.J.M.).

23 July 1996; accepted 26 September 1996

Molar Tooth Diversity, Disparity, and Ecology in Cenozoic Ungulate Radiations

Jukka Jernvall, John P. Hunter,* Mikael Fortelius†

A classic example of adaptive radiation is the diversification of Cenozoic ungulates into herbivore adaptive zones. Their taxonomic diversification has been associated with changes in molar tooth morphology. Analysis of molar crown types of the Artiodactyla, Perissodactyla, and archaic ungulates ("Condylarthra") shows that the diversity of genera and crown types was high in the Eocene. Post-Eocene molars of intermediate crown types are rare, and thus the ungulate fauna contained more taxa having fewer but more disparate crown types. Taxonomic diversity trends alone give incomplete descriptions of adaptive radiations.

Mammals are today the dominant terrestrial vertebrate group using plants as food (*1*). Mammalian herbivory has evolved independently numerous times during the past 65 million years (*2*). Along with rodents, ungulates are the most taxonomically diverse group of herbivorous mammals, both today and in the geologic past (*1*). The taxonomic diversification of ungulates, starting in the Paleocene, was associated with distinct changes in dental morphology (*1*–*3*), but the evolution of morphologies associated with herbivory is only incidentally correlated with phylogenetic groupings (*4*). Ecomorphological groupings that cut across phylogenetic boundaries should be used to study the rise of herbivory (*2*, *5*). Teeth offer good opportunities to link morphology to ecology through diet. Here we develop criteria to classify mammalian molar shapes and thus connect taxonomic and morphological diversity in ungulates through the Cenozoic.

We tabulated each morphological type of upper second molar as a discrete crown type (*6*). The crown type classification is a phylogenetically neutral scheme in which cusp shape, number, and location as well as

J. Jernvall, Institute of Biotechnology and Department of Ecology and Systematics, Post Office Box 56, 00014 University of Helsinki, Finland, and Department of Anthropology, State University of New York at Stony Brook, Stony Brook, NY 11794–4364, USA.
J. P. Hunter, Department of Anatomical Sciences, State University of New York at Stony Brook, Stony Brook, NY 11794–8081, USA.
M. Fortelius, Palaeontology Division, Finnish Museum of Natural History, Post Office Box 11, 00014 University of Helsinki, Finland.

*Present address: Department of Anatomy, New York College of Osteopathic Medicine, Old Westbury, NY 11568, USA.
†Present address: Division of Geology and Palaeontology, Department of Geology, University of Helsinki, Post Office Box 11, FIN-00014 University of Helsinki, Finland.

SCIENCE

29 NOVEMBER 1996
VOL. 274 • PAGES 1